- -

Possible Roles of Spontaneous Waves and Dendritic Growth for Retinal Receptive Field Development

- -

Burgi, Pierre-Yves; Grzywacz, Norberto M.

Possible Roles of Spontaneous Waves and Dendritic Growth for Retinal Receptive Field Development

Pierre-Yves Burgi
Norberto M. Grzywacz
Smith-Kettlewell Eye Research Institute,
San Francisco, CA 94115 USA

Several models of cortical development postulate that a Hebbian process fed by spontaneous activity amplifies orientation biases occurring randomly in early wiring, to form orientation selectivity. These models are not applicable to the development of retinal orientation selectivity, since they neglect the polarization of the retina's poorly branched early dendritic trees and the wavelike organization of the retina's early noise. There is now evidence that dendritic polarization and spontaneous waves are key in the development of retinal receptive fields. When models of cortical development are modified to take these factors into account, one obtains a model of retinal development in which early dendritic polarization is the seed of orientation selectivity, while the spatial extent of spontaneous waves controls the spatial profile of receptive fields and their tendency to be isotropic.

1 Introduction _____

Retinal cells display some functionally mature receptive fields as soon as light responses can be recorded, even prior to birth or eye opening (Masland, 1977; Rusoff & Dubin, 1977; Dacheux & Miller, 1981a, 1981b; Tootle, 1993; Sernagor & Grzywacz, 1995a). In some species, early ganglion cells are even selective to the orientation of image features and the direction of their motion (Masland, 1977; Sernagor & Grzywacz, 1995a). These selectivities may in some sense be genetically specified. However, as it was well expressed by Jacobson (1991), "How essentially the same gene products form a brain [structure] at one position and a spinal cord [another structure] at another place is not given directly by the genome, but eventuates from a network of regulatory epigenetic processes." When applied to the retina, this reasoning leads to an interest in epigenetic processes that contribute to the retina's receptive field self-organization.

Three observations may be key to the understanding of the development of retinal orientation selectivity. First, in the retina, complex receptive field properties such as orientation selectivity seem to depend on a single synaptic

layer (the inner plexiform layer, IPL) (Dowling, 1987). Second, developing retinas are characterized by early polarization of dendritic trees (Maslim, Webster, & Stone, 1986; Ramoa, Campbell, & Shatz, 1988; Dunlop, 1990; Vanselow, Dutting, & Thanos, 1990), which seems to impart anisotropies to immature receptive fields (Sernagor & Grzywacz, 1995a). Third, multi-electrode and optical recording studies in developing retinas of cats and ferrets have revealed that waves of neural activity propagate in random directions across the ganglion cell surface and the IPL (Meister, Wong, Baylor, & Shatz, 1991; Wong, Meister, & Shatz, 1993), correlating the activity of neighbor amacrine and ganglion cells (Wong, Chernjavsky, Smith, & Shatz, 1995). Such a correlation in retinal neighbor cells has also been observed in other species (in rat, Maffei and Galli-Resta, 1990; in turtle, Sernagor & Grzywacz, 1993).

It has been shown that self-organizing multilayer networks with random uncorrelated noise in the first layer, retinotopic connections (with random errors) from layer to layer, and Hebb-like rules for synaptic maturation can lead to the emergence of orientationally selective cells with similar properties to those in the cortex (von der Malsburg, 1973; Linsker, 1986; Yuille, Kammen, & Cohen, 1989; Miller, 1994).

We now report the results of substituting retinal-like connections and noise for those used to simulate cortical development. We demonstrate that when Linsker's (1986) model of self-organization of receptive fields is modified to incorporate spontaneous waves (see Fig. 1A) and early dendritic polarization (see Fig. 1B), the spatial extent of the former controls the spatial profile of receptive fields and their tendency to be isotropic and the latter introduces a bias that helps the development of orientation selectivity. (The material described in this article has appeared in abstract form as Burgi & Grzywacz, 1994a.)

2 Modification of Linsker's Model to Include Waves and Polarized Dendrites

Linsker's model (1986) consists of a multilayer network with feedforward connections. Following MacKay and Miller's analysis of Linsker's model (1990), we consider two layers (besides, possibly, an input layer). The density of synapses from cells in layer A (for amacrine, in our later discussion) to a given cell in the next ascending layer G (for ganglion) assumes a gaussian distribution as function of the position of the cells in layer A. Variations in synaptic strength during development are described by a quadratic Hebb-type rule. For a given set of activities in layer A, such as determined by spontaneous uncorrelated noise or waves, this rule expresses the variations in synaptic weight ω_i of synapse i as a function of its activity F_i^A and the overall activity F^G of the postsynaptic cell. Synaptic maturation is described
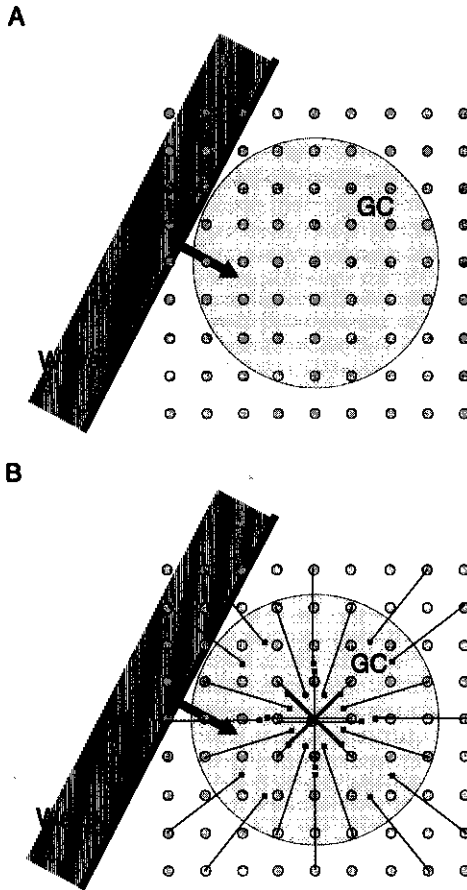
Figure 1: Two models of the developing inner plexiform layer (IPL). The ganglion cell dendritic tree, represented as a hatched circle, receives synaptic connections from (A) "dendritic-less" amacrine cells (small circles) or (B) amacrine dendrites (straight lines ending on black squares, which represent the synapses). The position of the synapses is random and follows a gaussian distribution concentric with the ganglion cell's dendritic tree. The dendrodendritic amacrine processes are assumed to originate at the amacrine cell's soma and point toward the ganglion cell's soma. Waves of activity, one of which is shown propagating from top left to bottom right, are modeled by an infinitely extended straight wave front with a gaussian profile of depolarization perpendicular to the direction of propagation. The waves propagate through the IPL and correlate the activity of neighbor cells. This correlation depends on the distance separating two cells, the waves' direction of propagation, and the orientation of the dendritic processes.

by the following dynamical equation (Linsker, 1986),

$$\frac{d}{dt}\omega_i = c_1 + \sum_j (\underline{Q}_{ij}^A + c_2)\, D_j \omega_j, \tag{2.1}$$

where $\underline{Q}_{ij}^A = \overline{(F_i^A - \overline{F^A})(F_j^A - \overline{F^A})}$ is the covariance matrix (the overbars denote average and $\overline{F^A} = \overline{F_i^A} = \overline{F_j^A}$), D_j is synaptic density, $c_1 = k - F_0^G(\overline{F^A} - F_0^A)$, and $c_2 = \overline{F^A}(\overline{F^A} - F_0^A)$, with F_0^G, F_0^A, and k being constants of the Hebbian rule. In this and next sections, we consider the case $c_1 = c_2 = 0$ to compare the outcomes of equation 2.1 for different covariance matrices. In section 4 we analyze the behavior of the system in the $c_1 - c_2$ plane.

For the original Linsker model, the noise in the layer preceding layer A is uncorrelated and random, and the arbor of connections between these layers is gaussian. Therefore, the covariance function Q_u in layer A has a gaussian form (Linsker, 1986). We define σ_u to denote its spatial standard deviation.

For comparison with the Linsker model, we calculated what the covariance function would be if the noise assumed the form of spontaneous waves in layer A instead of uncorrelated noise (see the appendix for details). We recently proposed a biophysical model for the generation and propagation of spontaneous waves of activity in the developing retina (Burgi & Grzywacz, 1994b, 1994c), based on pharmacological results (Sernagor & Grzywacz, 1993). As an approximation to the waves in the model, they were modeled here by an infinitely extended straight wave front with a gaussian profile of depolarization along the direction of propagation. In this case, by assuming the synaptic response at each instant to be proportional to the wave-induced depolarization on the amacrine cell, one obtains in the continuum limit (for details, see the appendix),

$$Q_\omega(\vec{r}, \vec{r}') = e^{-\Delta^2/8\sigma_\omega^2} I_0(\Delta^2/8\sigma_\omega^2), \tag{2.2}$$

where $\vec{r}$ and $\vec{r}'$ are two vectors originating at the target cell in layer G (for us, a ganglion cell) and ending at two cells in layer A (for us, amacrine cells), $\Delta = |\vec{r} - \vec{r}'|$, σ_ω denotes the spatial standard deviation of the waves, and $I_0(x)$ is the zero-order Bessel function of an imaginary argument.

Finally, we obtained the covariance function for the case of waves exciting the ganglion cell via polarized amacrine dendrites. The dendrite was modeled as a straight process, with a synapse at one ending of this process contacting the ganglion cell in a random position in this cell's dendritic tree (see Fig. 1B). For simplicity, an arrow beginning at the middle of the amacrine dendrite and ending at its synapse always pointed toward the center of the ganglion cell's tree. The synaptic response at each instant was taken to be proportional to the integral of the wave-induced depolarization

along the length of the dendrite. The covariance function was computed as the mean covariance due to waves moving in all possible directions. This function is (see the appendix for details),

$$Q_d(\vec{r}, \vec{r}') = \int_{|\vec{r}|}^{|\vec{r}|+L} \int_{|\vec{r}'|}^{|\vec{r}'|+L} \exp\left(-\frac{\Delta_{x'x''}^2}{8\sigma_\omega^2}\right) I_0\left(\frac{\Delta_{x'x''}^2}{8\sigma_\omega^2}\right) dx'\, dx'', \qquad (2.3)$$

where $\vec{r}$ and $\vec{r}'$ are vectors originating at the ganglion cell soma and ending at amacrine synapses, $\Delta_{x'x''} = |x'\vec{u}_r - x''\vec{u}_r'|$, with $\vec{u}_r$ and $\vec{u}_r'$ being unit vectors in the direction of $\vec{r}$ and $\vec{r}'$, respectively, and L is the length of the amacrine dendrite.

For the three covariance functions, we assumed the synaptic density function to the ganglion cell to be a gaussian distribution of standard deviation σ_s, that is,

$$D(\vec{r}') = e^{-|\vec{r}'|^2/2\sigma_s^2}. \qquad (2.4)$$

This distribution reflects the dendritic arbor of the ganglion cell.

3 Eigenvector Analysis

To determine what kinds of receptive field emerge from these models, one must solve equation 2.1. For this purpose, the covariance functions were first discretized on square lattices (size 17×17). Next, to obtain all possible outcomes of equation 2.1, we calculated the eigenvalues and eigenvectors of matrix $(Q_{ij}^A + c_2)D_j$ (the general solution is a linear combination of the fundamental solution set $\{e^{\lambda_1 t}\vec{u}_1, e^{\lambda_2 t}\vec{u}_2, \cdots, e^{\lambda_n t}\vec{u}_n\}$, where λ_i is the eigenvalue corresponding to the eigenvector $\vec{u}_i$ and the coefficients of the linear combination are determined by the initial conditions, plus a term corresponding to a particular solution of the nonhomogeneous equation). Inspection of equations 2.2–2.4, as well as Linsker's covariance function, reveals that the parameter space involves only the spatial spread of the arbor to the amacrine layer in Linsker's model (σ_u), the wave's width (σ_ω), the dendritic length (L), and the synaptic density spread (σ_s). Because these parameters have the dimensions of space, it is possible to study the general behavior of the solutions of these equations with only three dimensionless parameters, by scaling σ_u, σ_ω, and L by σ_s, the constant in the three models. To allow a direct comparison between Linsker's model and our two-layer models, we assumed $\sigma_u = \sigma_\omega = \sigma$. Hence, the only free parameters left to explore were σ/σ_s and L/σ_s.

To determine the eigenvalues and eigenvectors that solve equation 2.1, we applied the transformation $t_j = D_j^{1/2}\omega_j$, which symmetrizes the ma-

trix $Q_{ij}^A D_j$ (MacKay & Miller, 1990). The symmetrized matrix was then transformed into a tridiagonal matrix using Householder reduction, and the eigenvalues and eigenvectors were obtained using the QL algorithm (Wilkinson & Reinsch, 1971).

If one assumes (see also MacKay & Miller, 1990) that the synaptic weights must stop growing at some point, then the final receptive fields will tend to be dominated by the eigenvectors with the highest eigenvalues. This domination would not be absolute; variations among cells will occur because of initial random variations in wiring. Initial wiring and termination of development are complex processes, which may depend, for example, on transient gene expression of particular proteins or immature morphologies of dendritic trees. Consequently, to prevent obscuring the main points of the article, we decided to omit the detailed mathematical and computational analyses of the outcome given various initial conditions and termination rules. Accordingly, our results, expressed in terms of eigenvalues and eigenvectors, should be interpreted only as *tendencies* for symmetry breaking of the different covariance functions, and not as final incidences of various cell-types.

The principal eigenfunctions in all three models (for $c_1 = c_2 = 0$) were found to be circularly symmetrical, and symmetry breaking could occur only if the next eigenfunction in line dominated by random chance (see Fig. 2). To measure the affinity of the network for symmetry breaking, we considered the ratio between the largest and second-largest eigenvalues. This ratio was high for Q_ω (in comparison to Linsker's original model; see Fig. 2A). The ratio became even higher as we widened the waves. The physical reason for this tendency is that wide waves tend to correlate the activity of many amacrine cells, thus averaging out local statistical orientational biases that might exist by chance in the retinal wiring.

The ratio between the two largest eigenvalues was smaller when dendrites were present than when they were not. Moreover, the symmetrical center-surround eigenvector that was in the second position for Q_u and Q_ω was relegated to the fourth position for Q_d, behind two anisotropic eigenfunctions (see Fig. 2C). Taken together, these two changes indicate that dendritic polarization biases the system toward symmetry breaking, facilitating the formation of orientationally selective cells.

Although the three sets of eigenfunctions corresponding to Q_u, Q_ω, and Q_d resemble each other visually (see Fig. 2), they are not identical. For Linsker's case, the eigenfunctions of Q_u have been derived analytically by MacKay and Miller (1990). Although we could not do so for Q_ω and Q_d due to the Bessel function, we could verify that the analytic expressions of their eigenfunctions differ from those of Q_u. It is possible to see these differences reflected in the eigenfunctions. For instance, the main eigenfunctions are flatter for waves (the larger central white area) than for uncorrelated noise. Similarly, changes between positive and negative regions of the other
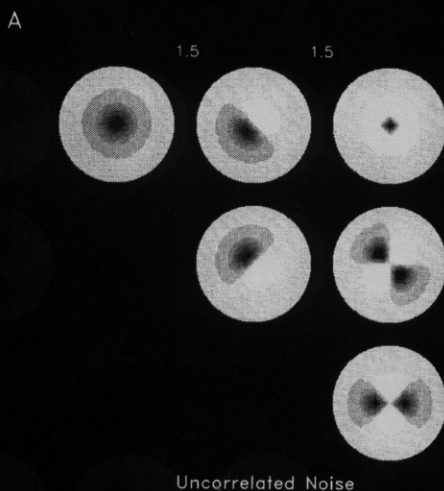
A

Uncorrelated Noise

Figure 2: Principal eigenfunctions of the covariance functions. The three cases illustrated in this figure correspond to the original Linsker model with uncorrelated noise (A), to a modification of that model, substituting spontaneous waves for uncorrelated noise (B), and to a modification of that model using both waves and polarized dendritic inputs (C). In each column, the eigenfunctions have the same eigenvalue, the column with the largest eigenvalue being at the left. The ratio between every two successive eigenvalues is indicated by the number between every two columns. The gray-scale bar is proportional to synaptic strength. Each eigenfunction has been normalized to use the full gray scale. Parameters were $\sigma_\omega = 20\,\mu$m (Burgi & Grzywacz, 1994c), $\sigma_u = 20\,\mu$m, $\sigma_s = 50\,\mu$m, and $L = 60\,\mu$m (Kolb, 1982). While the left-most eigenfunctions represent concentric receptive fields that will be favored by the model, the next receptive fields in line are orientationally selective. Other simulations with σ_ω, σ_s, and L ranges of 12–100 μm, 10–80 μm, and 25–200 μm, respectively, were performed with similar results. In comparison to development with waves only, development with dendritic polarization helps symmetry breaking. *Continued following page.*

eigenfunctions are faster for uncorrelated noise than for waves. The wave eigenfunctions are flatter because of the "infinite" extent of the waves' fronts, which coordinates cells over large distances.

How variations in σ_ω/σ_s and amacrine dendritic length affect the tendency for symmetric eigenfunctions (estimated by λ_1/λ_2) is shown in Figure 3. Large σ_ω/σ_s, corresponding to either wide waves or narrow synaptic density distributions, were found to favor concentric cells (see Fig. 3A). This
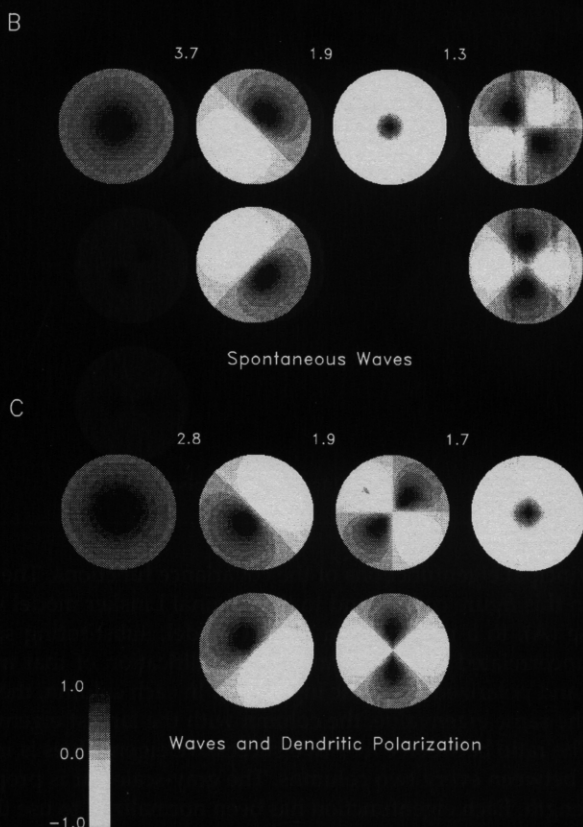
Figure 2: *Continued.*

result is consistent with wide waves (wide with respect to σ_s), tending to synchronize the activity of large groups of cells whatever the wave's directions of propagation. A similar interpretation can be given for uncorrelated random noise where a wide arbor of connections between layer A and the layer preceding it smoothes out local statistical biases for orientation selectivity present in the wiring, leading to more symmetry (see Fig. 3A). The effect of dendritic length on symmetry breaking is shown in Figure 3B. The value of λ_1/λ_2 decreases as dendritic length increases, with the largest variations for lengths smaller or comparable to the spatial spread of the waves. Therefore, larger dendritic lengths help symmetry breaking. For very small dendritic lengths, λ_1/λ_2 becomes equivalent to the case without dendrites.

A

B
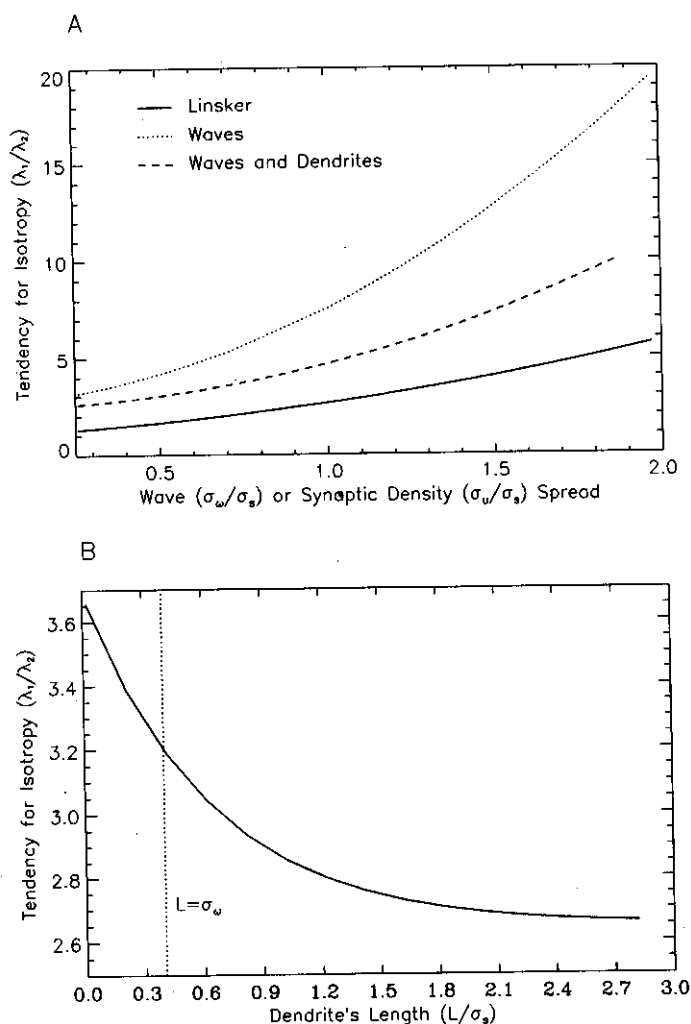
Figure 3: Effects of parameter variations on symmetry breaking. (A) The tendency for isotropy expressed as λ_1/λ_2 is plotted against the spatial spread (σ_u) of the arbor at the input to the amacrine cells (for the original Linsker model) or the spatial spread (σ_w) of the waves along the direction of their propagation (for the models substituting waves for uncorrelated noise). These plots are either in the presence or absence of polarized dendritic inputs ($L/\sigma_s = 1.2$) to the ganglion cell. (B) The ratio λ_1/λ_2 is plotted against dendritic length for $\sigma_w/\sigma_s = 0.4$. The results show that symmetry breaking becomes more likely as the size of the amacrine dendrites grows and as the spreads of the waves and arbor at the input to the amacrine cells diminish.

Finally, how variations in the waves' width and amacrine dendritic length affect the shape of the eigenfunctions is illustrated in Figure 4. For waves of spatial spread four times wider than those used in Figure 2B, we found the same set of eigenfunctions, but more spatially extended (roughly 2.5 times more extended; see Fig. 4A). Consequently, the spatial extent of the waves may be important not only for controlling the tendency of formation of concentric receptive fields, but also may contribute to their spatial extent. (In support, there is now evidence that spontaneous waves are key to the determination of receptive field size during retinal development; Sernagor & Grzywacz, 1994, 1995a, 1995b, 1996.) In turn, although increases in receptive field size were small when dendritic length was doubled (see Fig. 4B), the order of importance of the eigenfunctions changed. The center-surround eigenfunction was removed from the set of the first six eigenfunctions (see Fig. 2C), being replaced by three-angular-nodes anisotropic eigenfunctions reminiscent of immature receptive fields with multi-axes anisotropy as observed in embryonic turtle retina (Sernagor & Grzywacz, 1995a).

4 Analysis of Behavior in the $c_1 - c_2$ Plane

The parameters c_1 and c_2 depend on the choice of the Hebbian thresholds (F_0^G and F_0^A) and the average activity in layer A ($\overline{F^A}$). (In our models, this average activity is fixed by the waves' properties, that is, their spatial extent, speed, and frequency of occurrence.) While parameter c_2 affects the eigenvalues of the matrix $(\underline{Q}_{ij}^A + c_2)D_j$, parameter c_1 moves the fixed point of the dynamics with respect to the origin. Because $\underline{Q}_{ij}^A = \overline{(F_i^A - \overline{F^A})(F_j^A - \overline{F^A})}$, the entries of this matrix depend on both its spatial properties (determined by $i - j$) and the overall level of activity (determined by $\overline{F^A}$). But although the effects of the spatial properties of $\underline{Q}_{ij}^A$ are the central theme of this article, the square of the overall level of activity, which is proportional to the entries of $\underline{Q}_{ij}^A$, has the same dimensions as c_2. Therefore, it is possible to study the general behavior of the eigenvalues of $(\underline{Q}_{ij}^A + c_2)D_j$ with a single dimensionless parameter by scaling c_2 by the maximum of $\underline{Q}_{ij}^A$. Because this scaling is equivalent to normalizing the maximum of $\underline{Q}_{ij}^A$ ($\underline{Q}_{ii}^A$) to 1, in effect, we will be considering the correlation matrices instead of the covariance ones.

The parameter c_1 does not affect the eigenvalues of $(\underline{Q}_{ij}^A + c_2)D_j$. Rather, it affects the coefficients of the linear combination of $\{e^{\lambda_1 t}\vec{u}_1, e^{\lambda_2 t}\vec{u}_2, \ldots, e^{\lambda_n t}\vec{u}_n\}$ in the solution of equation 2.1. The effect on these coefficients is such that if the magnitude of c_1 is large, then it gives a significant head start to the all-excitatory (all-inhibitory) profiles. Feng, Pan, and Roychowdhury (1995) analyzed how this head start would affect the outcome of the evolution of equation 2.1 if the synaptic weights were constrained to lie between fixed
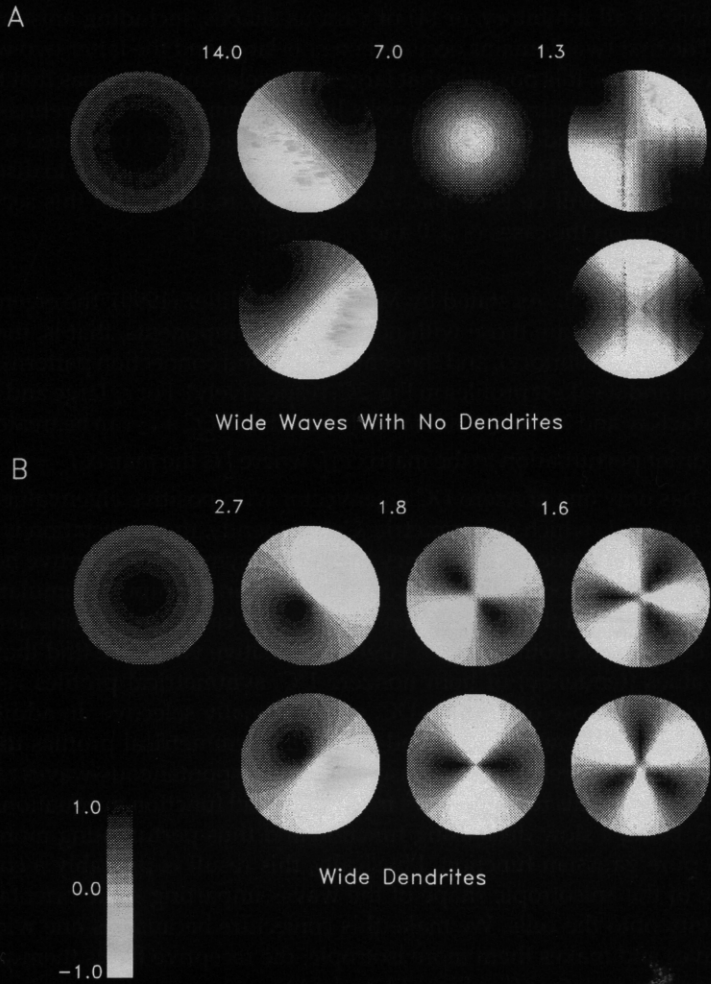
Figure 4: Effects of parameter variations on eigenfunctions. Parameters are the same as in Figure 2, except that in (A) waves' width is 80 μm and in (B), amacrine dendritic length is 120 μm. Comparison of A with Figure 2B shows that the width of the receptive field grows with the width of the waves. Comparison of B with Figure 2C shows that the width of the receptive field grows with the length of the amacrine dendrites.

minimum and maximum values. These authors reached the conclusion that
the stable fixed-point solutions to the equation would lie in four domains
where receptive-field profiles are (1) all excitatory, (2) all inhibitory, (3) all
excitatory or all inhibitory, or (4) of various shapes, including anisotropic
ones. The first two domains occur when c_1 is large and the latter two when
it is close to zero. It is possible that large c_1 are relevant for retinas that have
a majority of concentric ganglion cells like the primate and cat retinas. (In
section 5, we will address how surround inhibition may be added to all-
excitatory profiles.) However, if c_1 is large, there is nothing more to discuss;
receptive fields will be isotropic. Consequently, in the rest of this section,
we will focus on the cases $c_2 > 0$ and $c_2 < 0$ for $c_1 = 0$.

The Case $c_2 > 0$. As stated by MacKay and Miller (1990), the eigenvec-
tors affected by c_2 are those with nonzero DC components, that is, the all-
excitatory (all-inhibitory), and the center-surround connection patterns (the
strongest and weakest profiles in Fig. 2C, respectively). For c_2 large and pos-
itive, MacKay and Miller (1990) have observed that $\underline{Q}^A_{ij} + c_2$ can be treated as
a first-order perturbation to the matrix $c_2\underline{J}$, where $\underline{J}$ is the matrix $\underline{J}_{ij} = 1$. This
matrix has only one nonzero DC eigenvector with positive eigenvalue: the
vector $\vec{n}$, $n_i = 1$, which is symmetric. Consequently, the expectation is that
as c_2 increases, so does the tendency to develop symmetric receptive fields.
A mathematical proof (MacKay & Miller, 1990) and computer simulations
(see Fig. 5) confirm this expectation for the three cases we are considering.
When c_2 increases from zero to a large and positive value, we find that the
eigenvalues (tendency) of both nonzero-DC, symmetrical profiles rise in
comparison to those of the non-DC, orientationally selective. In addition,
the simulations show that the tendency is for symmetrical profiles to rise
faster for the uncorrelated-noise case than for the spontaneous-waves cases.
Mathematically, this result follows from the Bessel function in equations 2.2
and 2.3, being a slow decreasing function and thus perturbating more $c_2\underline{J}$
than a pure gaussian function. Physically, this result is probably a conse-
quence of the anisotropic shape of the waves imparting more orientation
selectivity onto the cells. We make this conjecture because as one widens
the waves and makes them more isotropic, the receptive fields themselves
become more isotropic (see Figs. 3A and 4A).

The Case $c_2 < 0$. For c_2 large and negative, when one performs the
perturbation analysis, one finds that $c_2\underline{J}$ has anisotropic eigenvectors with
eigenvalues equal to zero and that its only nonzero-DC, symmetric eigen-
vector, $\vec{n}$, has a negative eigenvalue, which is proportional to c_2. As a result,
the eigenvalue of the all-excitatory (all-inhibitory) eigenvector becomes neg-
ative, making this receptive field essentially irrelevant (MacKay & Miller,
1990). Computer simulations also reveal that the eigenvalue of the center-
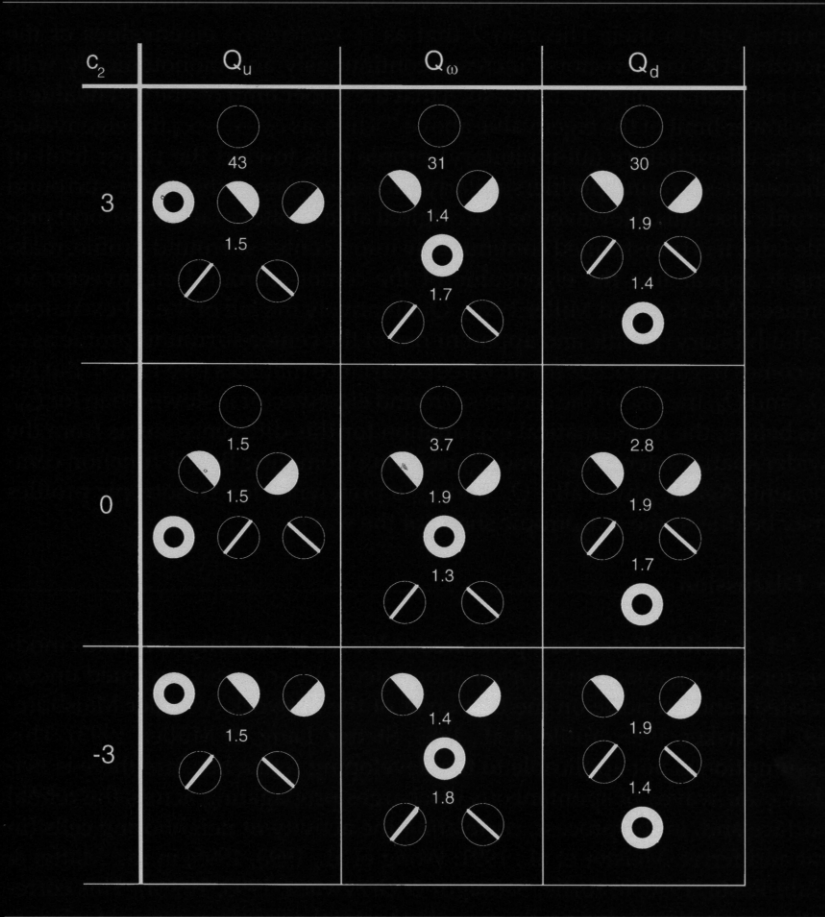surround eigenvector increases (and that of all other eigenvectors with

Figure 5: Effects of the parameter c_2 on eigenfunctions. All-excitatory (all-inhibitory) profiles are schematically represented by circles; center-surround by black annuli, one-axis anisotropy (second column of Fig. 4B) by half-white–half-black disks, and two-axis anisotropy (third column of Fig. 4B) by disks bisected by lines. The ordering of the profiles is like those in Figures 2 and 4, except the receptive fields here are arranged vertically, with the most important ones at the top. The parameters $\sigma_u, \sigma_\omega, \sigma_s$, and L are the same as in Figure 2. For large $|c_2|$, and respectively to waves, value of uncorrelated noise favors symmetrical receptive fields in comparison to spontaneous waves. In addition, this figure illustrates that the bias toward symmetry breaking resulting from dendritic polarization is independent of the choice of c_2.

nonzero-DC components) as c_2 decreases from zero to a large and negative value. This result was first observed by MacKay and Miller (1990), who pointed out in their Theorem 2 that as c_2 varies, the eigenvalues of the nonzero-DC eigenvectors "increase continuously and monotonically with (c_2) between asymptotic limits such that the upper limit of one eigenvalue is the lower limit of the eigenvalue above." Thus, as $c_2 \rightarrow -\infty$, the eigenvalue of the all-excitatory (all-inhibitory) profile falls toward the upper limit of the center-surround profile; similarly, the eigenvalue of the center-surround profile also falls. However, as the original all-excitatory (all-inhibitory) profile falls, it is transformed continuously into a center-surround profile, making it appear like the eigenvalue of the center-surround eigenvector increases (MacKay and Miller 1990). Qualitatively the fall of the all-excitatory (all-inhibitory) profile and apparent rise of the center-surround profile as c_2 becomes negative occur for all three covariance matrices (see Fig. 5). But for Q_ω and Q_d, the rise of the center-surround eigenvector is slower than for Q_u. As before, the mathematical explanation for this difference stems from the wider spatial extent of Q_ω and Q_d resulting from their Bessel-function component. Again, physically, Q_ω and Q_d's preference for anisotropic profiles may be due to the anisotropic shape of the waves.

5 Discussion

5.1 Possible Roles for Spontaneous Waves of Activity. Previous models for self-organization of orientation selectivity in cortex assumed uncorrelated random noise on the first layer of the network (von der Malsburg, 1973; Linsker, 1986; Yuille et al., 1989; Stetter, Lang, & Müller, 1993). This assumption is not applicable to the developing retina because there is evidence for waves of spontaneous discharges propagating across the retinal surface and, in the process, correlating the activity of neighboring cells (in cat and ferret: Meister et al., 1991; Wong et al., 1993, 1995; in rat: Maffei & Galli-Resta, 1990; in turtle, Sernagor & Grzywacz, 1993, 1995a). This correlation is observed during the period of retinal synaptogenesis (Maslim & Stone, 1986; Horsburgh & Sefton, 1987; De Juan, Grzywacz, Guardiola, & Sernagor, 1996), and dendritic growth and remodeling (Wong, Hermann, & Shatz, 1991; De Juan, Grzywacz, Guardiola, & Sernagor, 1995). Consequently, one must ponder on the role that these spontaneous correlating waves of activity may have in the formation of retinal receptive fields.

We modified one of the cortical models (Linsker's) to include waves and compared the tendencies for formation of particular types of receptive fields in the new and old models through an analysis of their covariance matrices. In this analysis, the likely types of receptive fields were described by these matrices' eigenvectors with highest eigenvalues, and the tendency of each type of receptive field to develop was estimated by the eigenvalues. The main eigenfunctions of the Linsker and wave-modified covariance matrices were found to have similar profiles. These profiles were purely excita-

tory concentric, orientationally selective, and excitatory-center–inhibitory-surround concentric. Wide waves tend to favor concentric receptive fields more than narrow waves (see Fig. 3A). The physical reason for the isotropy tendency of wide waves in the model is that their wide extent tends to correlate the activity of many amacrine cells, thus averaging out local statistical orientational biases that might exist by chance in the retinal wiring. Whether this averaging really favors isotropy may be debatable, since averaging also weakens the tendency for the center-surround profile (see Fig. 4A). In Figure 3, we used the all-excitatory profile to quantify isotropy, because in the retina, surround inhibition appears early in development, even before mature concentric or orientationally selective receptive fields emerge (Sernagor & Grzywacz, 1995a). This suggests that perhaps the inhibitory surround of center-surround profiles might be determined genetically, independent of spontaneous activity. If this suggestion is incorrect and the emergence of surround depends on spontaneous activity, then c_2 must be negative to eliminate the all-excitatory profile (see Fig. 5). In this case, that the early retinal noise comes in the form of waves would favor the formation of orientation selectivity. As discussed in section 4, this bias toward anisotropic profiles may be due to the anisotropic shape of the waves.

Another possible role for waves is contributing to the size of receptive fields. Waves tend to yield wider receptive fields than uncorrelated noise because of the large lateral extent of the wave fronts. In addition, wider waves tend to give rise to wider receptive fields (see Fig. 4A). This coupling between wave width and receptive field size could have implications for explaining receptive field size differences across species. Recent data are strongly supportive of the role of waves for both the formation of concentric receptive fields and control of their size. Normally, in turtle, the wavelike activity lasts until about postnatal day 21 (P21) and then disappears (Sernagor & Grzywacz, 1995a). Coincidentally with the disappearance of waves, the receptive field sizes mature (Sernagor & Grzywacz, 1995a). However, if one dark-rears the turtles, the wavelike activity is stronger and longer lasting (>P40), and the receptive fields become larger and more concentric (Sernagor & Grzywacz, 1994). Furthermore, the density of growth cones (and thus of dendritic growth) increases under dark rearing (De Juan et al., 1995). In turn, if one blocks the waves chronically by implanting in the retina curare-soaked Elvax (Elvax is an ethylene vinyl-acetate copolymer) (Sernagor & Grzywacz, 1995b, 1996), the receptive fields stop growing and become less concentric. Although there are other explanations for the changes in receptive field size and concentricity with dark rearing and curare implantation, these changes are generally consistent with our model.

5.2 Possible Roles for Early Dendritic Polarization. To mimic the polarization of poorly branched dendritic trees of immature cells (Maslim et al., 1986; Ramoa et al., 1988; Dunlop, 1990; Vanselow et al., 1990), we modified the original Linsker model to include (waves and) amacrine dendritic

processes pointing toward the ganglion cell's soma and making contact
with its dendritic tree. We then applied the covariance-matrix analysis to
this case. The ratio between the two largest eigenvalues of the resulting
covariance matrix was found to be smaller than for the model with only
waves (see Fig. 3A), and this effect was more pronounced for longer den-
drites (see Fig. 3B). Moreover, for long dendrites, the eigenfunction order
changed as the center-surround concentric eigenfunctions were relegated to
a less dominant position than anisotropic ones (see Figs. 2C and 4B). These
results indicate that dendritic polarization biases the system toward orien-
tation selectivity. Such a bias was also suggested by Sernagor and Grzywacz
(1995b), who found physiological correlates of the dendritic polarization in
immature retinas.

Appendix

This appendix shows the main steps for the derivation of equations 2.2
and 2.3. We want to determine how the activity of two amacrine cells is corre-
lated by spontaneous waves propagating through the amacrine layer. Waves
were modeled by an infinitely extended straight wave front and a gaussian
profile (of standard deviation σ_ω) along the direction of propagation. The
synaptic response at each instant was taken to be proportional to the value
of the wave on the amacrine cell, that is, $F^A(\vec{r}) \sim \exp\left(-(\vec{r} \cdot \vec{u}_\omega + x)^2/2\sigma_\omega^2\right)$,
where $\vec{r}$ is the vector originating at the ganglion cell soma and ending at
the amacrine cell, $\vec{u}_\omega$ is the unit vector in the direction of the wave's prop-
agation, and x is the shortest distance between the ganglion cell soma and
the wave's crest (see Fig. 6). The correlation between two amacrine cells can
thus be expressed as $Q(\vec{r}, \vec{r}') = \overline{F^A(\vec{r})F^A(\vec{r}')}$, where the overbar denotes aver-
age over a large number of waves and the prime refers to another amacrine
cell. The correlation was computed as the mean correlation due to waves
moving in all possible directions and spatial locations,

$$Q(\vec{r}, \vec{r}') = \int_{-\infty}^{\infty} \int_{-\pi}^{\pi} F^A(\vec{r})F^A(\vec{r}')dx\, d\theta, \tag{A.1}$$

where we are omitting the normalization factor and other constants from
the analysis as they only scale the eigenvectors. Developing equation A.1,
and taking into account the waves' symmetry, we get

$$Q(\vec{r}, \vec{r}') = \int_{-\infty}^{\infty} \int_{-\pi}^{\pi} \exp\left(-\frac{(|\vec{r}|\cos(\alpha - \theta) + x)^2}{2\sigma_\omega^2}\right)$$
$$\times \exp\left(-\frac{(|\vec{r}'|\cos(\alpha' - \theta) + x)^2}{2\sigma_\omega^2}\right) dx d\theta, \tag{A.2}$$

where α and α' are the vector orientations of $\vec{r}$ and $\vec{r}'$, respectively, and θ
is the wave's direction of propagation. After arranging the integrand as an
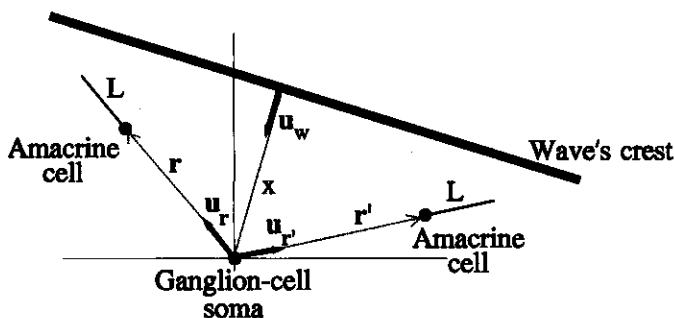
Figure 6: Schematic representation of the variables used to determine the wave's covariance functions. Two vectors $\vec{r}$ and $\vec{r}'$ (dashed arrows) originate at the ganglion cell soma (shown at the origin) and end at two amacrine synapses (represented by filled circles). The orientations of these vectors are represented by the unit vectors $\vec{u}_r$ and $\vec{u}_{r'}$. A wave propagates with a direction represented by the unit vector $\vec{u}_w$ and has its peak amplitude (represented by a bold, straight line) at a distance x from the ganglion cell. The amacrine dendrites are shown as solid lines of length L.

exponential of a perfect square, the integral in x is straightforward and gives $\sigma_\omega \sqrt{\pi}/2$. As constants are omitted from the analysis, equation A.2 becomes

$$Q(\vec{r}, \vec{r}') \sim \int_{-\pi}^{\pi} \exp\left(-\frac{\left(|\vec{r}|\cos(\alpha - \theta) - |\vec{r}'|\cos(\alpha' - \theta)\right)^2}{4\sigma_\omega^2}\right) d\theta. \quad (A.3)$$

Using trigonometric manipulations, it can be shown that

$$\left(|\vec{r}|\cos(\alpha - \theta) - |\vec{r}'|\cos(\alpha' - \theta)\right)^2 = |\vec{r} - \vec{r}'|^2 \cos^2(\theta - \gamma), \quad (A.4)$$

where $\gamma = tg^{-1}(|\vec{r}|\sin\alpha - |\vec{r}'|\sin\alpha')/(|\vec{r}|\cos\alpha - |\vec{r}'|\cos\alpha')$. Using this definition and the new variable $\phi = \theta - \gamma$ (the integral limits does not change as γ is an arbitrary angle), equation A.3 can be integrated with respect to ϕ (Gradshteyn & Ryzhik, 1980) to yield

$$Q(\vec{r}, \vec{r}') \sim \exp\left(-\frac{|\vec{r} - \vec{r}'|^2}{8\sigma_\omega^2}\right) I_0\left(\frac{|\vec{r} - \vec{r}'|^2}{8\sigma_\omega^2}\right), \quad (A.5)$$

where $I_0(x)$ is the zero-order Bessel function of an imaginary argument.

For the calculation of the covariance function for waves hitting polarized dendrites, the dendrite was modeled as a straight process with a dendro-dendritic synapse contacting the ganglion cell in a random position in this cell's gaussian dendritic tree. An arrow beginning at the middle of the dendrite and ending at the synapse always pointed toward the middle of the ganglion cell tree. The synaptic response at each instant was taken to be proportional to the integral of the values of the wave along the length of the dendrite, that is,

$$F^A(\vec{r}) \sim \int_{|\vec{r}|}^{|\vec{r}|+L} \exp\left(-\frac{(\vec{u}_r \cdot \vec{u}_\omega \, x' + x)^2}{2\sigma_\omega^2}\right) dx', \tag{A.6}$$

where $\vec{u}_r$ is a unit vector in the direction of $\vec{r}$ and L is dendritic length (see Fig. 6). As before, the correlation between the activity of two amacrine cells, $F^A(\vec{r})$ and $F^A(\vec{r}')$, was computed as the mean correlation due to waves moving in all possible directions:

$$Q(\vec{r}, \vec{r}') = \int_{-\infty}^{\infty} dx \int_{-\pi}^{\pi} d\theta \int_{|\vec{r}|}^{|\vec{r}|+L} \exp\left(-\frac{(\cos(\alpha - \theta) \, x' + x)^2}{2\sigma_\omega^2}\right) dx'$$
$$\times \int_{|\vec{r}'|}^{|\vec{r}'|+L} \exp\left(-\frac{(\cos(\alpha' - \theta) \, x'' + x)^2}{2\sigma_\omega^2}\right) dx''. \tag{A.7}$$

Integrating with respect to x and using the same trigonometric manipulations as before, we get

$$Q(\vec{r}, \vec{r}') \sim \int_{|\vec{r}|}^{|\vec{r}|+L} \int_{|\vec{r}'|}^{|\vec{r}'|+L} \exp\left(-\frac{\Delta_{x'x''}^2}{8\sigma_\omega^2}\right) I_0\left(\frac{\Delta_{x'x''}^2}{8\sigma_\omega^2}\right) dx' \, dx'' \tag{A.8}$$

where

$$\Delta_{x'x''} = |x'\vec{u}_r - x''\vec{u}_r'|.$$

Acknowledgments

References

Burgi, P.-Y., & Grzywacz, N. M. (1994a). Does prenatal development of ganglion-cell receptive fields depend on spontaneous activity and Hebbian processes? *Invest. Ophthalmol. Vis. Sci., 35*, 2126.

Burgi, P.-Y., & Grzywacz, N. M. (1994b). Model based on extracellular potassium for spontaneous synchronous activity in developing retinas. *Neural Computation, 6*, 981–1002.

Burgi, P.-Y., & Grzywacz, N. M. (1994c). Model for the pharmacological basis of spontaneous synchronous activity in developing retinas. *J. Neurosci., 14*, 7426–7439.

Dacheux, R. F., & Miller, R. F. (1981a). An intracellular electrophysiological study of the ontogeny of functional synapses in the rabbit retina. I. Receptors, horizontal and bipolar cells. *J. Comp. Neurol., 198*, 307–326.

Dacheux, R. F., & Miller, R. F. (1981b). An intracellular electrophysiological study of the ontogeny of functional synapses in the rabbit retina. II. Amacrine cells. *J. Comp. Neurol., 198*, 327–334.

De Juan, J., Grzywacz, N. M., Guardiola, J. V., & Sernagor, E. (1995). Anatomical and physiological dark-rearing induced changes in turtle retinal development. *Invest. Ophthalmol. Vis. Sci., 36*, 60.

De Juan, J., Grzywacz, N. M., Guardiola, J. V., & Sernagor, E. (1996). Coincidence of synaptogenesis and emergence of spontaneous and light-evoked activity in embryonic turtle retina. *Invest. Ophthalmol. Vis. Sci., 37*, 634.

Dowling, J. E. (1987). *The retina.* Cambridge, MA: Harvard University Press.

Dunlop, S. A. (1990). Early development of retinal ganglion cell dendrites in the marsupial *setonix brachyurus*, quokka. *J. Comp. Neurol., 293*, 425–447.

Feng, J., Pan, H., & Roychowdhury, V. P. (1995). *Linsker-type Hebbian learning: A quantitative analysis on the parameter space* (Tech. Rep. No. TR-EE 95-12). Purdue University.

Gradshteyn, I. S., & Ryzhik, I. M. (1980). *Table of integrals, series, and products.* Orlando, FL: Academic Press.

Horsburgh, G. M., & Sefton, A. J. (1987). Cellular degeneration and synaptogenesis in the developing retina of the rat. *J. Comp. Neurol., 263*, 553–566.

Jacobson, M. (1991). *Developmental neurobiology.* New York: Plenum Press.

Kolb, H. (1982). The morphology of the bipolar cells, amacrine cells and ganglion cells in the retina of the turtle *Pseudemys scripta elegans. Philos. Trans. R. Soc. B, 298*, 355–393.

Linsker, R. (1986). From basic network principles to neural architecture: Emergence of orientation-selective cells. *Proc. Natl. Acad. Sci. USA, 83*, 8390–8394.

MacKay, D. J. C., & Miller, K. D. (1990). Analysis of Linsker's application of Hebbian rules to linear networks. *Network, 1*, 257–297.

Maffei, L., & Galli-Resta, L. (1990). Correlation in the discharges of neighboring rat retinal ganglion cells during prenatal life. *Proc. Natl. Acad. Sci. USA, 87*, 2861–2864.

Masland, R. H. (1977). Maturation of function in the developing rabbit retina. *J. Comp. Neurol., 175*, 275–286.

Maslim, J., & Stone, J. (1986). Synaptogenesis in the retina of the cat. *Brain Research, 373*, 35–48.

Maslim, J., Webster, M., & Stone, J. (1986). Stages in the structural differentiation of retinal ganglion cells. *J. Comp. Neurol., 373*, 35–48.

Meister, M., Wong R. O. L., Baylor, D. A., & Shatz, C. J. (1991). Synchronous bursts of action potentials in ganglion cells of the developing mammalian retina. *Science, 252*, 939–943.

Miller, K. D. (1994). A model for the development of simple cell receptive fields and the ordered arrangement of orientation columns through activity-dependent competition between ON- and OFF-center inputs. *J. Neurosci., 14*, 409–441.

Ramoa, A. S., Campbell, G., & Shatz, C. J. (1988). Dendritic growth and remodelling of cat retinal ganglion cells during fetal and postnatal development. *J. Neurosci., 8*, 4239–4261.

Rusoff, A. C., & Dubin, M. W. (1977). Development of receptive-field properties of retinal ganglion cells in kittens. *J. Neurophysiol., 40*, 1188–1198.

Sernagor, E., & Grzywacz, N. M. (1993). Cellular mechanisms underlying spontaneous correlated activity in the turtle embryonic retina. *Invest. Ophthalmol. Vis. Sci., 34*, 1156.

Sernagor, E., & Grzywacz, N. M. (1994). Role of early spontaneous activity and visual experience in shaping complex receptive field properties of ganglion cells in the developing retina. *Neurosci. Abst., 20*, 1470.

Sernagor, E., & Grzywacz, N. M. (1995a). Emergence of complex receptive field properties of ganglion cells in the developing turtle retina. *J. Neurophysiol., 73*, 1355–1364.

Sernagor, E., & Grzywacz, N. M. (1995b). Shaping of receptive field properties in developing retinal ganglion cells in the absence of early cholinergic spontaneous activity. *Neurosci. Abst., 21*, 1503.

Sernagor, E., & Grzywacz, N. M. (1996). Influence of spontaneous activity and visual experience on developing retinal fields. *Current Biology, 6*, 1503–1508.

Stetter, M., Lang, E. W., & Müller, A. (1993). Emergence of orientation selective simple cells simulated in deterministic and stochastic neural networks. *Biol. Cybern., 68*, 465–476.

Tootle, J. S. (1993). Early postnatal development of visual function in ganglion cells of the cat retina. *J. Neurophysiol., 69*, 1645–1660.

Vanselow, J., Dutting, D., & Thanos, S. (1990). Target dependence of chick retinal ganglion cells during embryogenesis: Cell survival and dendritic development. *J. Comp. Neurol., 295*, 235–247.

von der Malsburg, C. (1973). Self organization of orientation selective cells in the striate cortex. *Kybernetik, 14*, 85–100.

Wilkinson, J. H., & Reinsh, C., (1971). *Linear algebra*. New York: Springer-Verlag.

Wong, R. O. L., Herrmann, K., & Shatz, C. J. (1991). Remodeling of retinal ganglion cell dendrites in the absence of action potential activity. *J. Neurobiol., 22*, 685–697.

Wong, R. O. L., Meister, M., & Shatz, C. J. (1993). Transient period of correlated bursting activity during development of the mammalian retina. *Neuron, 11*, 923–938.

Wong, R. O. L., Chernjavsky, A., Smith, S. J., & Shatz, C. J. (1995). Early functional neural networks in the developing retina. *Nature, 374,* 716–718.

Yuille, A. L., Kammen, D. M., & Cohen, D. (1989). Quadrature and the development of orientation selective cortical cells by Hebb rules. *Biol. Cybern., 61,* 183–194.